JOURNAL OF VIROLOGY, May 2010, p. 4124–4135 Vol. 84, No. 9
0022-538X/10/$12.00 doi:10.1128/JVI.02319-09

Herpes Simplex Virus 1 Regulatory Protein ICP27 Undergoes a Head-to-Tail Intramolecular Interaction▽†

Felicia P. Hernandez and Rozanne M. Sandri-Goldin*

Department of Microbiology and Molecular Genetics, School of Medicine, University of California, Irvine, California 92697

Received 2 November 2009/Accepted 9 February 2010

Herpes simplex virus type 1 (HSV-1) regulatory protein ICP27 is a multifunction functional protein that interacts with many cellular proteins. A number of the proteins with which ICP27 interacts require that both the N and C termini of ICP27 are intact. These include RNA polymerase II, TAP/NXF1, and Hsc70. We tested the possibility that the N and C termini of ICP27 could undergo a head-to-tail intramolecular interaction that exists in open and closed configurations for different binding partners. Here, we show by bimolecular fluorescence complementation (BiFC) assays and fluorescence resonance energy transfer (FRET) by acceptor photobleaching that ICP27 undergoes a head-to-tail intramolecular interaction but not head-to-tail or tail-to-tail intermolecular interactions. Substitution mutations in the N or C termini showed that the leucine-rich region (LRR) in the N terminus and the zinc finger-like region in the C terminus must be intact for intramolecular interactions. A recombinant virus, vNC-Venus-ICP27, was constructed, and this virus was severely impaired for virus replication. The expression of NC-Venus-ICP27 protein was delayed compared to ICP27 expression in wild-type HSV-1 infection, but NC-Venus-ICP27 was abundantly expressed at late times of infection. Because the renaturation of the Venus fluorescent protein results in a covalent bonding of the two halves of the Venus molecule, the head-to-tail interaction of NC-Venus-ICP27 locks ICP27 in a closed configuration. We suggest that the population of locked ICP27 molecules is not able to undergo further protein-protein interactions.

ICP27 is a multifunctional regulatory protein that is required for herpes simplex virus type 1 (HSV-1) infection. ICP27 interacts directly with a number of proteins in performing its many roles. At early times after infection, ICP27 interacts with a splicing protein-specific kinase, SRPK1, and recruits this predominantly cytoplasmic kinase to the nucleus, where ICP27 then interacts with members of a conserved family of splicing factors termed SR proteins (37, 43). Through these interactions, ICP27 mediates the aberrant phosphorylation of SR proteins, which, as a consequence, are unable to perform their roles in spliceosome assembly, resulting in an inhibition of host cell splicing (37). Also at early times after infection, ICP27 interacts with cellular RNA polymerase II (RNAP II) (49) through the C-terminal domain (CTD) and helps to recruit RNAP II to viral transcription/replication sites (10). As infection progresses, ICP27 disassociates from splicing speckles and interacts with the TREX complex mRNA export adaptor protein Aly/REF and recruits Aly/REF to viral replication compartments (5, 6). While associated with replication compartments, ICP27 binds viral RNA (8, 35) and, beginning about 5 h after infection, ICP27 begins shuttling between the nucleus and cytoplasm (21, 35, 41), escorting its bound RNA cargo through the nuclear pore complex to the cytoplasm by a direct interaction with the cellular mRNA export receptor TAP/NXF1 (5, 6, 21). In the cytoplasm, ICP27 enhances the translation initiation of some viral mRNAs by an interaction with translation initiation factors (13–15). ICP27 also contributes to the formation of Hsc70-containing nuclear foci or virus-induced chaperone-enriched (VICE) domains (3), which are thought to function in the proteasomal degradation of misfolded and ubiquitinated proteins, thus executing nuclear protein quality control (25). ICP27 interacts with and relocalizes Hsc70 to these VICE domains (24). VICE domains have been shown to contain cellular chaperone proteins, including Hsc70, as well as components of the 26S proteasome (3, 24). ICP27 also has been shown to interact with ICP8 when it is associated with RNAP II (30). Other direct interactions of ICP27 that have been reported include splicing factor SAP145 (2) and hnRNP K and CK2 (45).

The functional domains of ICP27 that are required for a number of its interactions have been mapped. ICP27 binds RNA through an RGG box RNA binding motif from amino acids 138 to 152 (8, 26, 35). The RGG box is also the region required for its interaction with SRPK1 (37), and this interaction is regulated by arginine methylation within the RGG box at arginines 138, 148, and 150 (42, 43). The interaction of Aly/REF with ICP27 includes the N-terminal region from amino acid 104 to 153 (6). The interaction of ICP27 with SR proteins and with ICP8 requires the C-terminal zinc finger-like region from amino acid 450 to the C terminus at amino acid 512 (30, 37). The interaction of ICP27 with three cellular proteins, RNAP II, TAP/NXF1, and Hsc70, requires that both the N-terminal leucine-rich region (LRR) and the C-terminal zinc finger-like region be intact (5, 10, 24).

A number of cellular proteins have been shown to undergo interactions of their N and C termini in a reversible manner that regulates their activities or protein interactions. These include zyxin, an adhesion protein that regulates actin assembly (27); myosin VIIA, an unconventional myosin that has ATPase activity

* Corresponding author. Mailing address: Department of Microbiology and Molecular Genetics, School of Medicine, Medical Sciences, B240, University of California, Irvine, CA 92697-4025. Phone: (949) 824-7570. Fax: (949) 824-9054. E-mail: rmsandri@uci.edu.

† Supplemental material for this article may be found at http://jvi.asm.org/.

▽ Published ahead of print on 17 February 2010.

(44); the scaffold protein PDZK1 (22); talin, a large, integrin-associated cytoskeletal protein (33); the membrane-associated Na^+/H^+ exchanger regulatory factor NHERF1/EBP50 (28); kinesin, a motor protein (11, 46); and Raf kinase, which is involved in regulating the mitogen-activated protein kinase (MAPK) pathway (7). Head-to-tail interaction generally results in a negative regulation of the protein's interactions with other proteins or the regulation of its activity. An HSV-1 protein, UL9, also has been shown to undergo head-to-tail interactions but as a dimer, not as a monomer (4). This interaction appears to modulate the DNA binding activity of the C terminus of UL9. Because head-to-tail intramolecular interaction would alter protein conformation, such interactions may serve as another mechanism for regulating protein interactions. ICP27 undergoes many protein-protein interactions in a somewhat temporally regulated manner. We have shown that arginine methylation and phosphorylation regulate ICP27's interactions with several of its binding partners (9, 43), and we propose that ICP27 undergoes head-to-tail intramolecular interactions to regulate its interactions with proteins that have been shown to bind to ICP27 only if both the N and C termini are intact. In this report, we demonstrate by bimolecular fluorescence complementation (BiFC) assays (16, 19) and fluorescence resonance energy transfer (FRET) by acceptor photobleaching (18) that ICP27 undergoes an intramolecular head-to-tail interaction.

MATERIALS AND METHODS

Cells, recombinant plasmids, and viruses. Rabbit skin fibroblasts (RSF) and Vero cells were grown on minimal essential medium supplemented with 10% fetal bovine serum. Vero 2-2 cells, an ICP27 complementing cell line, were grown in minimal essential medium supplemented with 10% fetal bovine serum containing 750 μg/ml G418 as described previously (40). Plasmids were constructed that contained the ICP27 gene fused to the N-terminal half (amino acids 1 to 154) of Venus fluorescent protein (29) and yellow fluorescent protein (YFP) and/or the C-terminal half of Venus (amino acids 155 to 238) or YFP. To construct plasmid N-Venus$^{a.a.1\text{-}154}$/ICP27 (termed N-Venus/ICP27), pSG130B/S, which contains the wild-type ICP27 gene, was used (38). An XhoI site was engineered within the 5′-untranslated region (UTR) of the ICP27 gene, generating the plasmid N-XhoI/pSG130B/S using a QuikChange II site-directed mutagenesis kit from Stratagene. Sequences corresponding to amino acids 1 to 154 of the fluorescent protein Venus, kindly provided by Atsushi Miyawaki (29), were amplified by PCR using primers containing XhoI restriction sites with linker sequences, as described previously (16), for ligation into plasmid N-XhoI/pSG130B/S. The ICP27/C-Venus$^{a.a.155+}$ plasmid (termed ICP27/C-Venus) was created using plasmid pSG130B/S/C-EcoRI, which is derived from plasmid pSG130B/S. An EcoRI site was engineered to disrupt the stop codon of ICP27 at amino acid 512. Sequences for amino acids 155 to 238 of Venus were amplified by PCR using primers containing EcoRI restriction sites along with linker sequences (16, 29, 38) and ligated into pSG130B/S/C-EcoRI to generate ICP27/C-Venus. Plasmid ICP27/N-Venus$^{a.a.1\text{-}154}$ (termed ICP27/N-Venus) was created using plasmid pSG130B/S/C-EcoRI. Venus sequences corresponding to amino acids 1 to 154 were amplified by PCR with primers containing EcoRI restriction sites. To create the plasmid N-Venus$^{a.a.1\text{-}154}$/ICP27/C-Venus$^{a.a.155+}$ (termed N-Venus/ICP27/C-Venus), plasmid N-Venus/ICP27 was digested with AgeI and SgrAI, and the fragment that corresponds to nucleotides −65 to 490 of ICP27, including Venus amino acids 1 to 154, was ligated into plasmid ICP27/C-Venus after AgeI/SgrAI digestion. Plasmid N-YFP/ICP27/C-YFP was constructed similarly, except that YFP sequences were amplified by PCR from pEYFP-C1 (Clontech). Substitution mutations in plasmid N-Venus/ICP27/C-Venus were created using the QuikChange II site-directed mutagenesis kit from Stratagene according to the manufacturer's protocol. Forward and reverse primers used for site-directed mutagenesis are depicted below. The nucleotide substitutions are underlined: ICP27 C483, 488S, C CGC CAG GAG AGT TCG AGT CGT GTC AGC GAG TTG ACG G and G GCG GTC CTC TCA AGC TCA GCA CAG TCG CTC AAC TGC C; ICP27 L8, 11, 15A, C ATT GAT ATG GCA ATT GAC GCC GGC CTG GAC GCC TCC GAC AGC G and G TAA CTA TAC CGT TAA CTG CGG CCG GAC CTG CGG AGG CTG TCG C; ICP27 S16, 18A, GGC CTG GAC CTC GCC GAC GCC GAT CTG GAC GAG and CCG GAC CTG GAG CGG CTG CGG CTA GAC CTG CTC. PCR primers for all other BiFC constructs are shown in Table S1 in the supplemental material.

For FRET analysis, the N-terminal cyan fluorescent protein (CFP)/ICP27 plasmid was constructed using a plasmid with an EcoRI site engineered within the 5′ UTR of the ICP27 gene, generating the plasmid pSG130B/S/N-EcoRI. Sequences for full-length enhanced CFP (ECFP) were amplified by PCR from pECFP-C1 (Clontech) using primers with EcoRI restriction sites for ligation into N-EcoRI/pSG130B/S. The C-terminal ICP27/YFP fusion construct was created by the ligation of sequences for full-length enhanced YFP (EYFP) that were amplified by PCR using plasmid pEYFP-C1 (Clontech) with primers containing EcoRI restriction sites into plasmid pSG130B/S/C-EcoRI. The N-terminal CFP/ICP27 and C-terminal ICP27/YFP fusion constructs were used to create the ICP27 fusion construct that expresses both CFP and YFP. The N-terminal CFP/ICP27 construct was cut with BamHI and SgrAI to release an N-terminal fragment that contained CFP. The same restriction enzyme digestion was performed for the C-terminal ICP27/YFP construct, and the N-terminal CFP fragment was ligated to create N-CFP/ICP27/C-YFP. All primers used in creating the constructs for FRET analysis are shown in Table S1 in the supplemental material. For TAP/NXF-1-CFP expression, TAP/NXF-1 was excised from the pGEXCS-TAP plasmid, kindly provided by Elisa Izaurralde (1), using the restriction enzymes NarI and BamHI, and was cloned within the AccI-BamHI sites of plasmid pECFP-C1 from Clontech.

HSV-1 strain KOS, ICP27 null mutants 27-LacZ (40) and 27-GFP (42), and vN-YFP/ICP27 (3) were described previously. To construct a recombinant virus expressing NC-Venus-ICP27, N-Venus/ICP27/C-Venus plasmid DNA and viral DNA isolated from 27-LacZ were cotransfected into Vero 2-2 cells (40). Homologous sequences within the 5′- and 3′-untranslated regions of ICP27 present in the plasmid DNA and viral DNA allowed the recombination and incorporation of N-Venus/ICP27/C-Venus into the viral genome. Plaques producing yellow fluorescence were isolated and plaque purified six times. The recombinant virus was termed vNC-Venus-ICP27.

BiFC. BiFC analysis was performed in transient transfection assays. The BiFC fusion constructs, N-Venus/ICP27/C-Venus, N-Venus/ICP27, ICP27/C-Venus, ICP27/N-Venus, N-Venus/ICP27 (L8A, L11A, L15A)/C-Venus, N-Venus/ICP27(C483, 488S)/C-Venus, and N-Venus/ICP27 (S16A, S18A)/C-Venus, were transfected into RSF cells grown in glass-bottom culture dishes (MatTek Corporation) using Lipofectamine 2000 by following the manufacturer's protocol. Eighteen hours after transfection, cells were infected at a multiplicity of infection (MOI) of 10 with 27-LacZ. Cells were viewed directly for fluorescence using a Zeiss LSM 510 Meta confocal microscope at a magnification of 63×.

FRET by acceptor photobleaching. Plasmid N-CFP/ICP27/C-YFP DNA or N-CFP/ICP27 and ICP27/C-YFP DNA was transfected into RSF cells. Cells were infected 24 h after transfection with 27-LacZ at an MOI of 10. Cells were fixed at 8 h after infection using 3.7% formaldehyde. CFP-YFP FRET by acceptor photobleaching was performed using an LSM 510 Meta confocal microscope to detect emission from CFP, excited at 458 nm, and YFP, excited at 514 nm, as described by Karpova and McNally (18). In this procedure, the acceptor protein, YFP, is photobleached at a specific location within the cell using the 514-nm laser line. The change in donor fluorescence is quantified by comparing prebleach and postbleach images. The FRET energy transfer efficiency (E_F) from at least 30 different bleached regions of interest was calculated using the formula $E_F = (I_{\text{postbleach}} - I_{\text{prebleach}})/I_{\text{postbleach}}$, where I is the average CFP fluorescence intensity after background subtraction. Quantification for FRET efficiency and percent FRET is shown in Table S2 in the supplemental material.

Immunofluorescence. RSF cells grown on glass coverslips were transfected with plasmid DNA from pSG130B/S expressing wild-type ICP27 and the ICP27-Venus fusion constructs as indicated in Fig. 3. Eighteen hours later, cells were infected with 27-LacZ at an MOI of 10. Cells were fixed at 4 and 8 h after infection using 3.7% formaldehyde. Cells were stained as described previously (10, 24) with either a Clontech Living Colors monoclonal antibody (632375) against GFP in the case of N-Venus/ICP27 and N-Venus/ICP27 (L8A, L11A, L15A) or an anti-ICP27 antibody (P1119; Virusys) in the case of ICP27/C-Venus, ICP27/N-Venus, N-Venus/ICP27 (C483S, C488S)/C-Venus, and wild-type ICP27. The GFP antibody recognizes an epitope that also is present in Venus. Cells were imaged using a Zeiss LSM 510 Meta confocal microscope at 63× magnification.

To visualize replication compartment formation during infection, RSF cells grown on glass coverslips were infected with HSV-1 KOS, vN-YFP/ICP27 (17), or vNC-Venus/ICP27 at an MOI of 5. Cells were fixed at 8 h after infection, and immunofluorescent staining was performed with anti-ICP27 antibody P1119 (Vi-

rusys), anti-ICP4 antibody P1101 (Virusys), or anti-RNA polymerase II antibody ARNA3 (Research Diagnostics). YFP and Venus fluorescence was viewed directly. Cells were imaged using a Zeiss LSM 510 Meta confocal microscope at 63× magnification.

For TAP/NXF1 overexpression, RSF cells grown in glass-bottom culture dishes were transfected with CFP-TAP/NXF-1. Twenty-four hours after transfection, cells were infected at an MOI of 5 with either HSV-1 KOS, vN-YFP/ICP27 (17), or vNC-Venus/ICP27, and cells were fixed at 8 and 12 h after infection. The localization of wild-type ICP27 during KOS infection was viewed using anti-ICP27 antibody P1119, which was directly labeled using the Zenon Texas Red-X Mouse IgG1 Labeling kit from Invitrogen. Venus, YFP, CFP, and Texas Red fluorescence were viewed using a Zeiss LSM 510 Meta confocal microscope at 63× magnification.

Competition experiment. RSF cells grown in glass-bottom culture dishes (MatTek Corporation) were transfected with plasmid DNA encoding N-Venus/ICP27/C-Venus or N-YFP/ICP27/C-YFP or cotransfected with N-Venus/ICP27 and ICP27/C-Venus. Twenty-four hours after transfection, cells were infected with HSV-1 KOS or 27-LacZ at an MOI of 10. Cells were viewed directly for fluorescence at 4 and 8 h after infection using an LSM 510 Meta confocal microscope at a magnification of 63×.

Western blot analysis. RSF were transfected with pSG130B/S, which encodes wild-type ICP27, or with plasmid NC-Venus/ICP27 and NC-Venus/ICP27(L8, 11, 15A), NC-Venus/ICP27(C483, 488S), or NC-Venus/ICP27(S16, 18A), or they were cotransfected with N-Venus/ICP27 and ICP27/C-Venus, ICP27/N-Venus and ICP27/C-Venus, or ICP27(C483, 488S)/C-Venus and ICP27/N-Venus, as indicated in Fig. 3. Twenty-four hours after transfection, cells either were mock infected or were infected with 27-LacZ for 8 h. Protein was harvested from cells by washing infected cell monolayers twice with cold phosphate-buffered saline (PBS) and then scraping the cells into 2× electrophoresis sample solution. For virus-infected cells, RSF cells were infected with HSV-1 KOS, vN-YFP-ICP27, and vNC-Venus-ICP27 at an MOI of 5 for 4, 8, and 12 h as indicated in Fig. 6. Proteins were fractionated by electrophoresis on SDS–10% polyacrylamide gels and were transferred to nitrocellulose. Membranes were probed as described previously (42, 43) with monoclonal antibodies against GFP (Living Colors 632375; Clontech), ICP27 (P1119), ICP4 (P1101), glycoprotein D (gD) (P1103; Virusys Corporation), glycoprotein C (gC) (P1104; Virusys Corporation), and β-actin (A5441; Sigma-Aldrich) as indicated.

One-step viral growth curves. Vero cells were infected with HSV-1 KOS, ICP27 null mutant 27-GFP (42), or vN-Venus/ICP27/C-Venus at an MOI of 1. Experiments were performed three times, and virus was harvested at 0, 4, 8, 16, and 24 h after infection. Plaque assays were performed on Vero cells.

RESULTS

ICP27 undergoes a head-to-tale intramolecular interaction. Recent studies have demonstrated a growing list of proteins whose activities and interactions are regulated through intramolecular associations, wherein a motif in a protein interacts with another motif in the same molecule (12, 31). ICP27 undergoes interactions with several proteins that require both the N and C termini of ICP27. To determine if ICP27 can associate with itself through head-to-tail intramolecular interaction, we used an approach called bimolecular fluorescence complementation, or BiFC (19, 20). In this approach, the yellow fluorescent protein (YFP) molecule is cut in half; and half is fused to one protein or domain of a protein of interest, and the other half is fused to another protein or domain of the protein. If the two proteins or two domains within the same protein come into direct contact, the two halves of the YFP molecule will come together and renature, and fluorescence will occur (20). The time of the renaturation of YFP is a rate-limiting step that takes several hours. Therefore, a variant of YFP, termed Venus, was developed (29). Venus has a fast and efficient renaturation time (39), and therefore we used Venus.

The N-terminal half of Venus was cloned onto the N terminus of ICP27, and the C-terminal half of Venus was fused to the C terminus of ICP27. Plasmid DNA from the resulting construct, N-Venus/ICP27/C-Venus, was transfected into RSF cells, and 24 h later cells were infected with the ICP27 null mutant virus 27-LacZ to activate the expression of the ICP27 promoter on N-Venus/ICP27/C-Venus by the action of VP16. At 4 and 8 h after infection, cells were viewed for fluorescence (Fig. 1). Venus fluorescence was seen clearly at 4 and 8 h after infection, indicating that intramolecular association had occurred (Fig. 1). In contrast, in cotransfections of two constructs in which the N-terminal half of Venus was fused to the N terminus of one molecule of ICP27 (N-Venus/ICP27) and the C-terminal half was fused to the C terminus of another molecule of ICP27 (ICP27/C-Venus), no fluorescence was detected (Fig. 1). This indicates that intermolecular head-to-tail interaction did not occur (Fig. 1). Further, intermolecular tail-to-tail interaction also did not occur, as seen in the cotransfection of constructs in which the N-terminal half of Venus was fused to the C terminus of one molecule of ICP27 (ICP27/N-Venus) and the C-terminal half of Venus was fused to the C terminus of another molecule of ICP27 (ICP27/C-Venus). To determine if the N-terminal leucine-rich region and the C-terminal zinc finger-like region of ICP27 must be intact for the intramolecular interaction to occur, substitution mutations were constructed. Leucine residues at positions 8, 11, and 15 in the N terminus were replaced with alanine (N-Venus/ICP27 L8A, L11A, L15A/C-Venus), and cysteine residues at positions 483 and 488 in the zinc finger domain were replaced with serine (N-Venus/ICP27 C483S, C488S/C-Venus). Little to no fluorescence was detectable in transfections with the leucine and cysteine substitution mutants (Fig. 1). The substitution of two serine residues adjacent to the leucine-rich region at positions 16 and 18 in the N terminus (N-Venus/ICP27 S16A, S114A/C-Venus) did not diminish Venus fluorescence (Fig. 1). We conclude that ICP27 undergoes a head-to-tail intramolecular interaction, and the N-terminal leucine-rich region and the C-terminal zinc finger region must be intact for this to occur.

We next performed immunofluorescent staining experiments and immunoblot analysis to ascertain that the reason for the lack of Venus fluorescence with the cotransfection of N-Venus/ICP27 and ICP27/C-Venus or ICP27/N-Venus and ICP27/C-Venus constructs was not due to the poor expression of these proteins or failure to localize to the nucleus. Plasmid DNA encoding wild-type ICP27, N-Venus/ICP27/C-Venus, N-Venus/ICP27, ICP27/C-Venus, ICP27/N-Venus, N-Venus/ICP27 C483S, C488S/C-Venus, and N-Venus/ICP27 L8A, L11A, L15A/C-Venus was transfected into RSF cells, which subsequently were infected with 27-LacZ for 4 and 8 h as indicated (Fig. 2). Wild-type ICP27 was stained with a monoclonal antibody to ICP27, as was ICP27/C-Venus and ICP27/N-Venus, to detect ICP27 expression (Fig. 2). Venus fluorescence was visualized directly for N-Venus/ICP27/C-Venus (Fig. 2). The Venus fusion masks the epitope in ICP27 recognized by the anti-ICP27 monoclonal antibody, and therefore N-Venus/ICP27, N-Venus/ICP27 C483S, C488S/C-Venus, and N-Venus/ICP27 L8A, L11A, L15A/C-Venus were stained with an anti-GFP antibody that recognizes an epitope also present in Venus. In all cases, the Venus fusion constructs were clearly expressed and localized to the nucleus.

To determine the levels of protein expression, cells were transfected with wild-type ICP27, N-Venus/ICP27/C-Venus, N-Venus/ICP27 L8A, L11A, L15A/C-Venus, N-Venus/ICP27

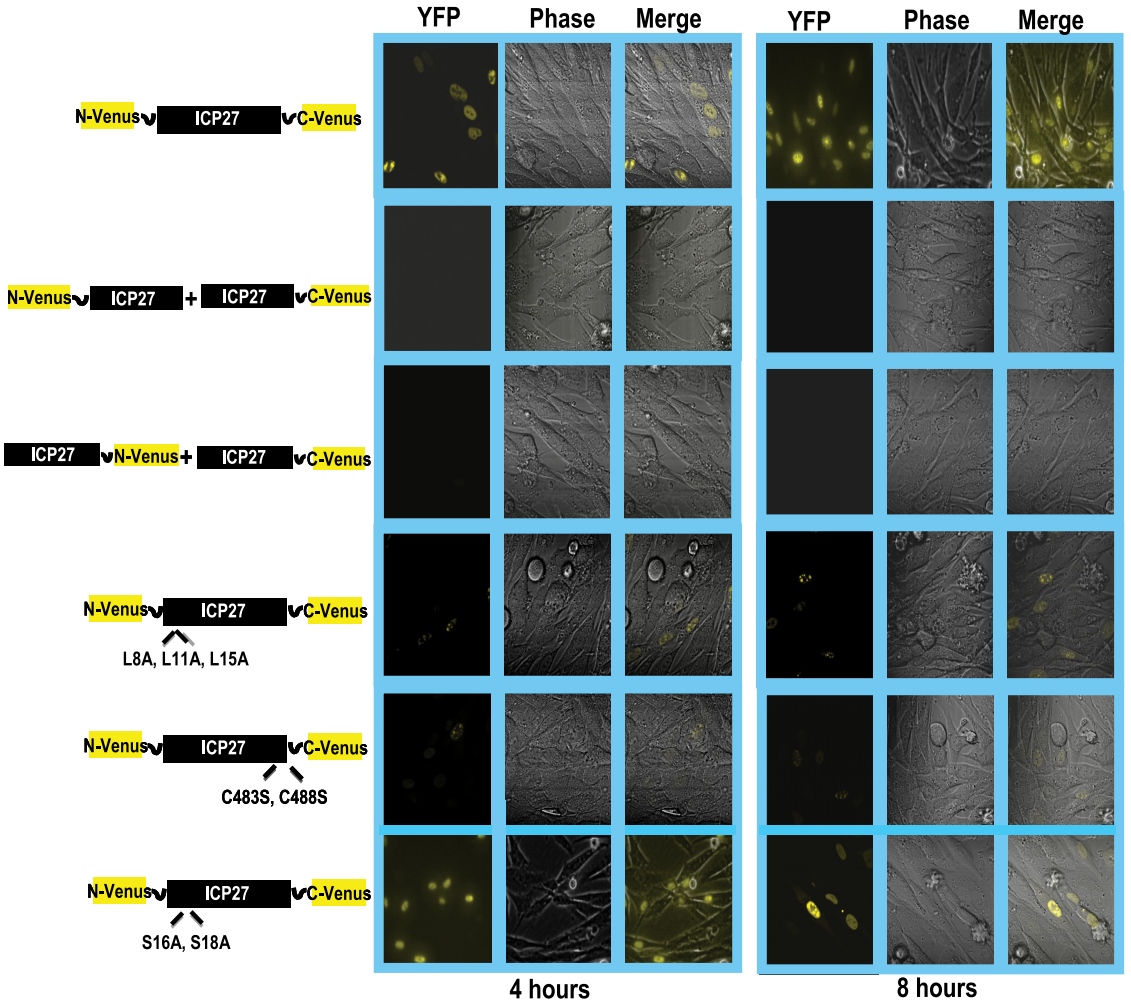

FIG. 1. BiFC analysis shows that ICP27 undergoes a head-to-tail intramolecular interaction. RSF cells were transfected with plasmid DNA from ICP27-Venus fusion constructs N-Venus/ICP27/C-Venus, N-Venus/ICP27 (L8A, L11A, L15A)/C-Venus, N-Venus/ICP27 (C483S, C488S)/C-Venus, and N-Venus/ICP27 (S16A, S18A) or were cotransfected with N-Venus-ICP27 and ICP27-C-Venus or with ICP27-N-Venus and ICP27-C-Venus as indicated. Eighteen hours after transfection, cells were infected with 27-LacZ at an MOI of 10. Venus fluorescence was visualized directly at 4 and 8 h after infection.

C483S, C488S/C-Venus, or N-Venus/ICP27 S16, S18A/C-Venus or were cotransfected with N-Venus/ICP27 and ICP27/C-Venus, ICP27/N-Venus and ICP27/C-Venus, or ICP27 C483S, C488S/C-Venus and ICP27/N-Venus. Twenty-four hours later, cells were infected with 27-LacZ for 8 h, at which time samples were harvested and Western blot analysis was performed with antibody to ICP27 and GFP as described above. N-Venus/ICP27 migrates more slowly than ICP27/C-Venus because of the protein linker that was used for the Venus fusion (Fig. 3). As seen in Fig. 3, the Venus fusion proteins were expressed at similar levels. Therefore, the lack of Venus fluorescence in the BiFC assay apparently was due to the lack of intermolecular interaction and not due to poor protein expression (Fig. 3) or improper localization (Fig. 2).

ICP27 intramolecular interaction was not competed for by wild-type ICP27. To determine if wild-type ICP27 could interact with N-Venus/ICP27/C-Venus to form a head-to-tail-dimer that might prevent BiFC and Venus fluorescence, cells were transfected with Venus and YFP constructs as depicted in Fig. 4. Eighteen hours later, cells were infected with HSV-1 KOS or 27-LacZ as a control. Venus and YFP fluorescence were visualized at 4 and 8 h after infection as indicated. BiFC was seen to occur for N-Venus/ICP27/C-Venus and for N-YFP/ICP27/C-YFP in KOS-infected cells, indicating that the presence of wild-type ICP27 did not interfere with the intramolecular interaction (Fig. 4). The number of cells showing Venus fluorescence for N-Venus/ICP27/C-Venus-transfected cells infected with KOS and 27-LacZ calculated from five fields, each containing around 50 cells, is shown in Table S2 in the supplemental material. There was no difference in BiFC seen between KOS- and 27-LacZ-infected cells. Further, the presence of wild-type ICP27 did not aid in the formation of an intermolecular interaction, because the cotransfection of N-Venus/ICP27 and ICP27/C-Venus showed no fluorescence (Fig. 4).

FRET by acceptor photobleaching confirmed that ICP27 undergoes head-to-tail intramolecular interaction but not intermolecular interaction. As another approach to analyze the ability of ICP27 to undergo an intramolecular interaction, we

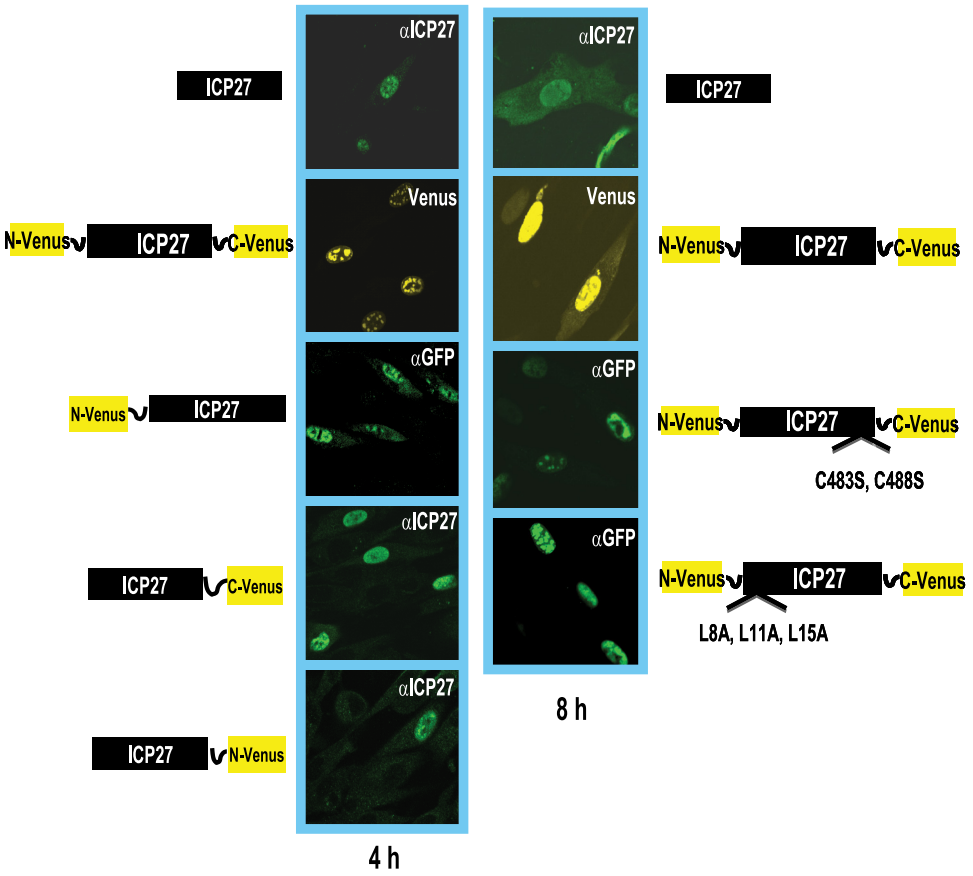

FIG. 2. Immunofluorescence analysis indicates that the ICP27-Venus fusion constructs are expressed and localized to the nucleus. RSF cells were transfected with plasmid DNA from a wild-type ICP27-containing plasmid and from the ICP27-Venus fusion constructs indicated. Eighteen hours after transfection, cells were infected with 27-LacZ at an MOI of 10 for 4 and 8 h as indicated. Wild-type ICP27 was stained with anti-ICP27 antibody P1119, as was ICP27-C-Venus and ICP27-N-Venus. N-Venus-ICP27, N-Venus/ICP27 (C483S, C488S)/C-Venus, and N-Venus/ICP27 (L8A, L11A, L15A)/C-Venus were stained with an anti-GFP antibody that recognizes an epitope also present in Venus. The P1119 anti-ICP27 antibody recognizes an epitope at the N terminus of ICP27 (23) that is masked by the N-Venus fusion protein. Venus yellow fluorescence was visualized directly for N-Venus/ICP27/C-Venus.

used FRET by acceptor photobleaching (18). CFP was fused to the N terminus of ICP27 and YFP was fused to the C terminus to create the construct CFP-ICP27-YFP. To determine if intermolecular interaction could occur, CFP was fused to the N terminus of one molecule of ICP27 (CFP-ICP27) and YFP was fused to the C terminus of another molecule (ICP27-YFP). Cells were transfected with CFP-ICP27-YFP or cotransfected with CFP-ICP27 and ICP27-YFP and were infected with 27-LacZ. At 8 h after infection, cells were imaged using an argon laser to detect CFP emission at 458 nm excitation and YFP emission at 514 nm. These images are labeled prebleach (Fig. 5). The bleaching of the acceptor protein YFP was performed using a 514-nm laser line at a specific location in the cell. The change in donor CFP fluorescence was quantified by comparing prebleach and postbleach images (Fig. 5). By this protocol, FRET is detected if donor fluorescence increases significantly more compared to what is detected in negative controls. Donor CFP fluorescence increased significantly upon bleaching (postbleach) in the CFP-ICP27-YFP samples (Fig. 5A and B), but FRET was not detected in the samples that were cotransfected with CFP-ICP27 and ICP27-YFP (Fig. 5C). FRET quantification is shown graphically in the right panels in Fig. 5, and the statistical analysis of FRET efficiency and percent FRET can be found in Table S3 in the supplemental material. The increase in donor fluorescence indicates a molecular interaction has occurred. FRET was seen for CFP-ICP27-YFP, indicating it was able to undergo a head-to-tail intramolecular interaction, but FRET was not detected for CFP-ICP27 and ICP27-YFP, indicating that intermolecular interaction did not occur.

Recombinant virus vNC-Venus-ICP27 is defective in viral replication. A recombinant virus, vNC-Venus-ICP27, was constructed in which N-Venus/ICP27/C-Venus was introduced into the viral genome in the ICP27 locus, replacing the ICP27 gene. Viral growth curves demonstrated that vNC-Venus-ICP27 was severely defective in viral replication, with growth in Vero cells being on par with an ICP27 null mutant virus 27-GFP (Fig. 6A). Venus fluorescence was viewed to confirm that the NC-Venus-ICP27 protein underwent an intramolecular interaction. Venus fluorescence was barely detectable at 4 h after infection but clearly was evident by 12 h after infection, indicating that the NC-Venus-ICP27 protein underwent a head-to-tail interaction (Fig. 6B). NC-Venus-ICP27 was predominantly nuclear even at 12 h after infection, whereas cytoplasmic fluorescence can be seen at 6 and 8 h for N-YFP-ICP27 ex-

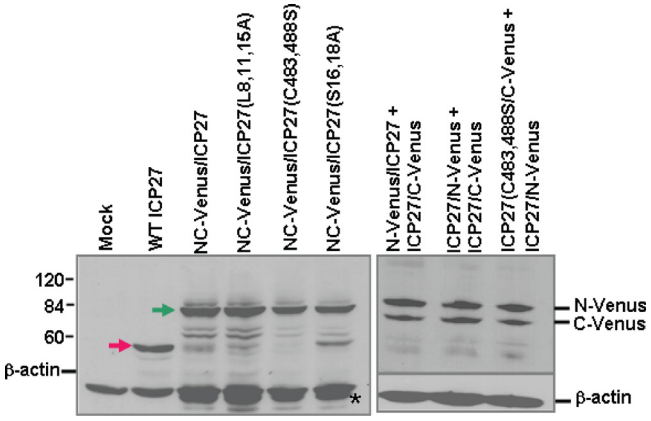

FIG. 3. ICP27-Venus fusion proteins are expressed to similar levels in transfected cells. RSF cells were transfected with the ICP27-Venus fusion constructs as indicated or with pSG130B/S, which expresses wild-type ICP27. Twenty-four hours later, cells were infected with 27-LacZ for 8 h, at which time samples were harvested. Western blot analysis was performed with anti-ICP27, anti-GFP, and anti-β-actin antibodies. The green arrow in the left panel points to the NC-Venus-ICP27 fusion proteins, and the red arrow points to wild-type ICP27. The positions of N-Venus/ICP27 and ICP27/C-Venus are indicated in the right panel. N-Venus/ICP27 migrates more slowly than ICP27/C-Venus because of the protein linker that was used in the construction of the N-Venus fusion protein. The asterisk in the left panel denotes a band that is likely a degradation product of the Venus-ICP27 fusion proteins and which migrated slightly faster than actin.

pressed by vN-YFP-ICP27 virus, as we reported previously (17). The virus vN-YFP-ICP27 replicates like wild-type KOS, as we showed previously (17). The delay in Venus fluorescence suggested that the expression of NC-Venus-ICP27 is delayed. Therefore, we monitored the expression of NC-Venus-ICP27 throughout infection by Western blot analysis (Fig. 6C). Wild-type ICP27 was detectable at 4 h after KOS infection and N-YFP-ICP27 was abundantly expressed at this time, but NC-Venus-ICP27 was not detected (Fig, 6C). However, NC-Venus-ICP27 was seen at 8 and 12 h after infection, although levels were lower than that for wild-type ICP27, indicating that expression is delayed compared to that of wild-type ICP27. The Western blot also demonstrated that NC-Venus-ICP27 protein migrated at around 95 kDa, which is similar in size to N-YFP-ICP27 (Fig. 6C), and was the size expected for the fusion of the N- and C-terminal halves of Venus to ICP27.

To determine viral protein expression during vNC-Venus-ICP27 infection, Western blot analysis was performed on samples isolated at 4, 8, and 12 h after infection (Fig. 6D). ICP4 levels were about 5-fold lower during vNC-Venus-ICP27 infection than during KOS and vN-YFP-ICP27 infection, whereas gC and gD levels were barely detectable (Fig. 6D). Therefore, viral gene expression during infection with vNC-Venus-ICP27 was severely reduced.

RNAP II is not recruited to viral replication compartments during infection with v-NC-Venus-ICP27. To determine where the block to viral replication occurs, we looked at the recruitment of RNAP II to viral transcription-replication sites, which

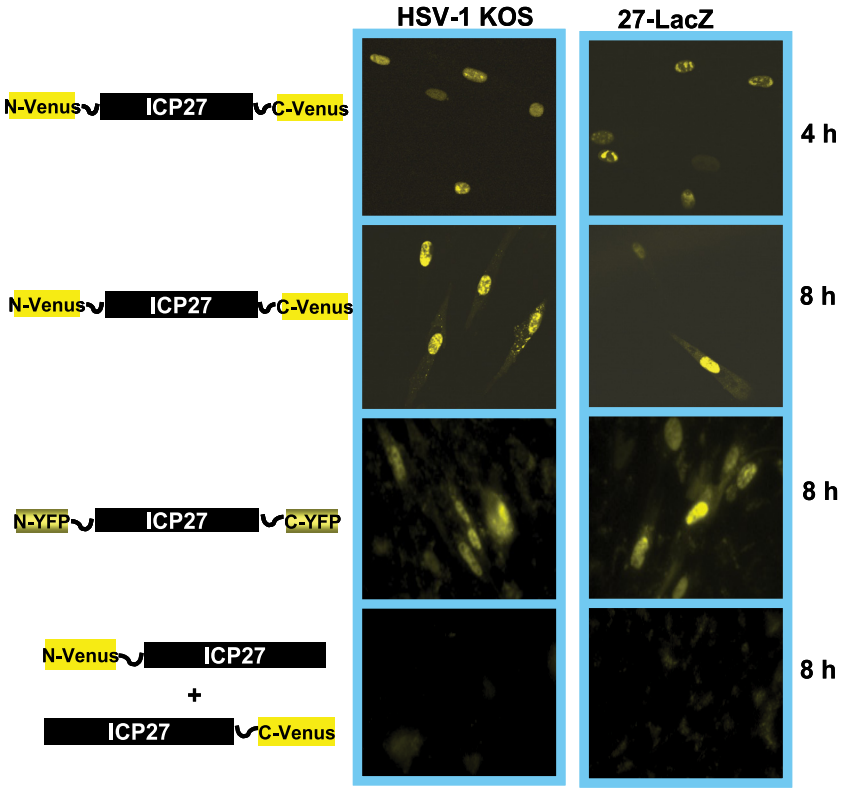

FIG. 4. ICP27 intramolecular interaction is not competed for by wild-type ICP27. RSF cells were transfected with N-Venus/ICP27/C-Venus or N-YFP/ICP27/C-YFP or were cotransfected with N-Venus-ICP27 and ICP27-C-Venus as indicated. Cells were infected 18 h later with HSV-1 KOS or 27-LacZ at an MOI of 10 for 4 and 8 h as indicated. Venus fluorescence was visualized directly.

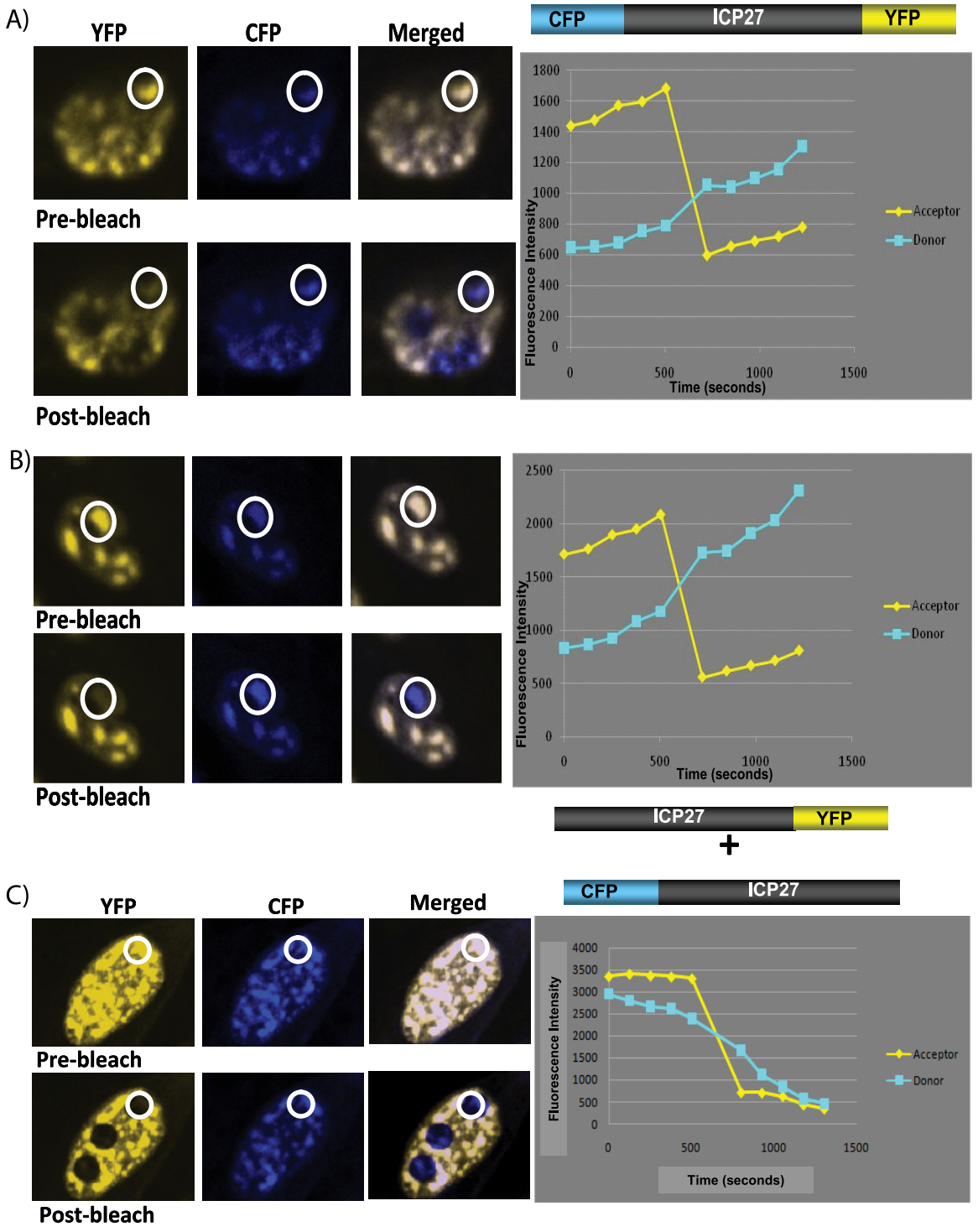

FIG. 5. FRET by acceptor photobleaching demonstrates that ICP27 undergoes a head-to-tail intramolecular interaction but not an intermolecular interaction. (A and B) RSF cells were transfected with N-CFP/ICP27/C-YFP DNA. Cells were infected 24 h after transfection with 27-LacZ at an MOI of 10. Cells were fixed at 8 h after infection. (C) RSF cells were transfected with N-CFP/ICP27 and ICP27/C-YFP DNA. Cells were infected 24 h after transfection with 27-LacZ at an MOI of 10. Cells were fixed at 8 h after infection. CFP-YFP FRET by acceptor photobleaching was performed using an LSM 510 Meta confocal microscope as described by Karpova et al. (18) and detailed in Materials and Methods. The white circles indicate the specific area within each cell that was bleached at 514 nm. FRET efficiency, which is plotted to the right of the fluorescent images, was calculated as follows: FRET (%) = 1 − (donor before bleach − background before bleach)/(donor after bleach − background after bleach) × 100.

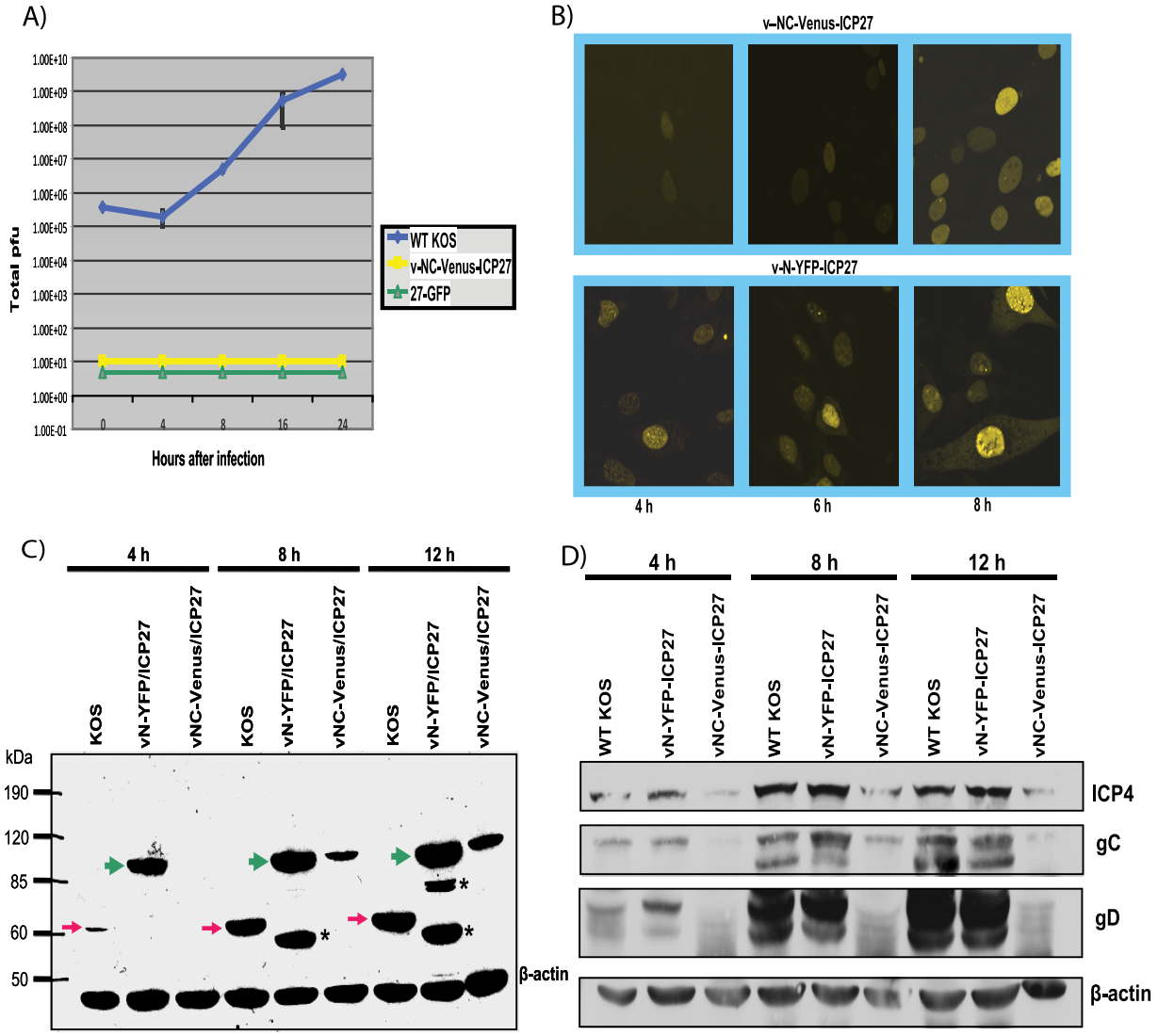

FIG. 6. Recombinant virus v-NC-Venus-ICP27 is defective in viral replication. The v-NC-Venus-ICP27 virus was constructed by the marker transfer of N-Venus/ICP27/C-Venus into 27-LacZ (40), replacing the 27-LacZ locus. (A) One-step growth curves were performed by infecting Vero cells with KOS, 27-GFP, and vNC-Venus-ICP27 at an MOI of 1. The experiments were performed in triplicate, and viral titers at 4, 8, 16, and 24 h were determined by plaque assays on Vero cells. (B) Vero cells were infected with v-NC-Venus-ICP27 and v-N-YFP-ICP27 at an MOI of 10. Venus and YFP fluorescence were visualized directly on living cells at 4, 6, and 8 h after infection. (C) Vero cells were infected with KOS, v-N-YFP-ICP27, and v-NC-Venus-ICP27 at an MOI of 10. Western blot analysis was performed on protein samples isolated at 4, 8, and 12 h after infection. The blot was probed with anti-ICP27 and anti-GFP antibodies and with β-actin antibody as a loading control. The red arrows indicate the position of wild-type ICP27. The green arrows indicate the position of N-YFP-ICP27 and N-Venus/ICP27/C-Venus. The asterisks denote ICP27 protein degradation products in the N-YFP-ICP27 lanes. The position of molecular size markers is shown to the left of the gel. (D) Vero cells infected with KOS, vN-YFP-ICP27, and v-NV-Venus-ICP27 at an MOI of 10 were harvested at 4, 8, and 12 h after infection, and Western blot analysis was performed as described previously (42). The blots were probed with antibodies directed to ICP4, gC, gD, and β-actin as a loading control.

requires ICP27 and which is an early event during infection (10, 32). ICP27 interacts with RNAP II through both its N and C termini, and the recruitment of RNAP II to viral replication sites is crucial for efficient viral transcription (10, 24). We also monitored the formation of viral replication compartments by staining for ICP4. Cells were infected with HSV-1 KOS, vN-YFP-ICP27, and vNC-Venus-ICP27. At 8 h after infection, cells were fixed and stained. ICP27 in KOS-infected cells was stained with anti-ICP27 antibody, and YFP and Venus fluorescence in vN-YFP-ICP27 and vNC-Venus-ICP27 infections was visualized directly (Fig. 7). RNAP II was seen in globular replication compartments in KOS- and vN-YFP-ICP27-infected cells, but a more diffuse nuclear fluorescence was seen for RNAP II in vNC-Venus-ICP27-infected cells (Fig. 7). This pattern resembled that of the cell that did not show Venus fluorescence in the nNC-Venus-ICP27 panels and that may represent an uninfected cell (Fig. 7). Further, while ICP4-containing viral replication compartments were seen in KOS- and vN-YFP-ICP27-infected cells, smaller prereplication sites were seen in vNC-Venus-ICP27-infected cells (Fig. 7). Thus,

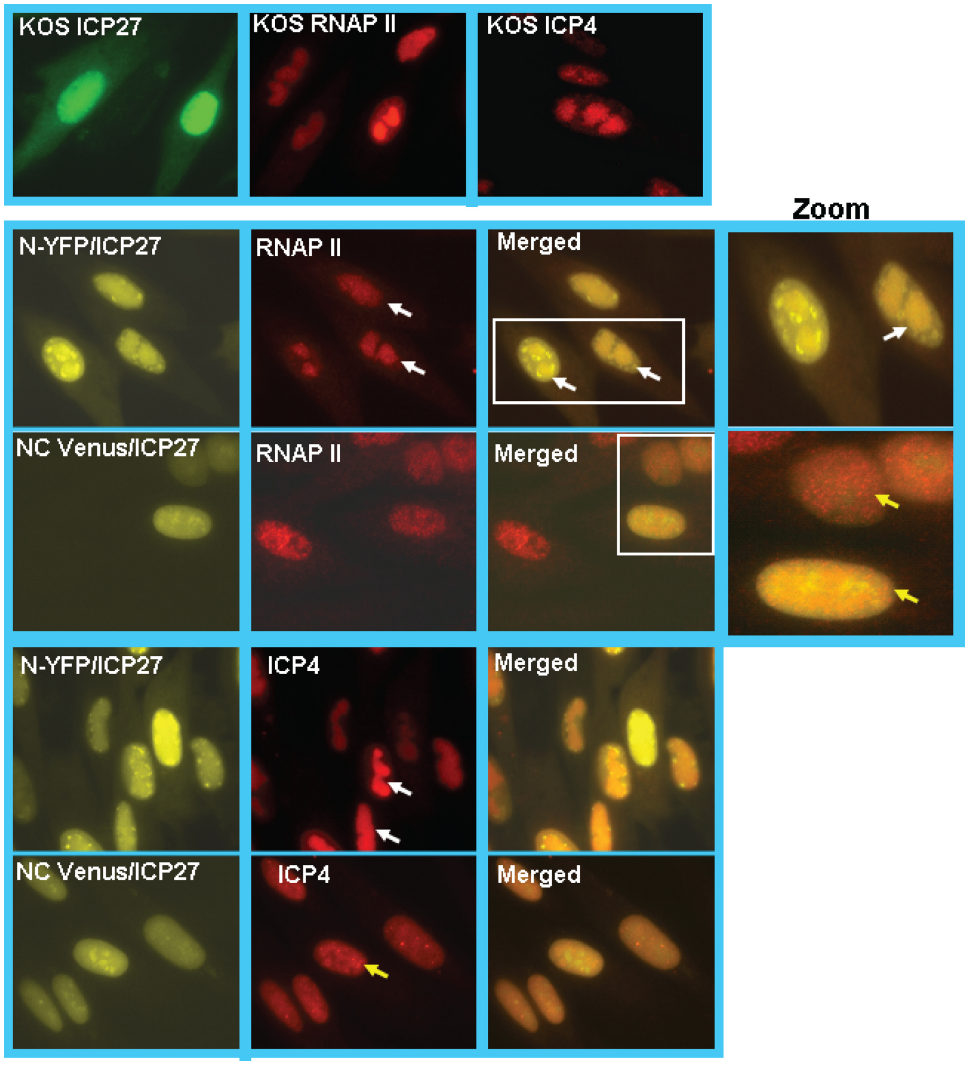

FIG. 7. Replication compartment formation is hindered during infection with v-NC-Venus-ICP27. RSF cells were infected with KOS, vN-YFP-ICP27, and v-NC-Venus-ICP27 at an MOI of 10 for 8 h, at which time cells were fixed. Immunofluorescent staining was performed with anti-ICP27 antibody for KOS-infected cells, anti-RNAP II antibody ARNA3, and anti-ICP4 antibody. YFP and Venus fluorescence was visualized directly. White rectangles indicate the region of the merged images that is shown in the zoomed images to the right. White arrows point to replication compartments, and yellow arrows point to small prereplication sites.

the recruitment of RNAP II and the formation of replication compartments were curtailed in infections with vNC-Venus-ICP27. Venus fluorescence was evident, indicating that BiFC occurred. Because the renaturation of Venus occurs through covalent interactions, molecules of ICP27 that are fluorescent are locked into the head-to-tail configuration. This may prohibit the interaction of ICP27 with RNAP II.

TAP/NXF1 overexpression causes export of NC-Venus-ICP27 to the cytoplasm. ICP27 interacts with TAP/NXF1 through both the N and C termini, and ICP27 shuttles to the cytoplasm through its interaction with TAP/NXF1 (5, 6, 17). During infection with vNC-Venus-ICP27 virus, ICP27 was nuclear predominantly at 8 and 12 h after infection (Fig. 6 and 7), at which times ICP27 is actively shuttling to the cytoplasm in KOS- and vN-YFP-ICP27-infected cells (Fig. 7). This suggests that NC-Venus-ICP27 is hindered in its interaction with TAP/NXF1. To determine what effect the overexpression of TAP/NXF1 might have on NC-Venus-ICP27 export, cells were transfected with CFP-TAP, in which TAP/NXF1 is under the control of the cytomegalovirus immediate-early promoter, and subsequently were infected with KOS, vN-YFP-ICP27, or vNC-Venus-ICP27 for 8 and 12 h. In KOS- and vN-YFP-ICP27-infected cells, ICP27 and N-YFP-ICP27 were notable in the cytoplasm at 8 and 12 h after infection both with and without TAP/NXF1 overexpression (Fig. 8). In the absence of TAP/NXF1 overexpression, NC-Venus-ICP27 remained nuclear at 8 and 12 h after infection; however, cytoplasmic fluorescence was detectable at 8 h and was clearly visible at 12 h after infection in cells transfected with CFP-TAP (Fig. 8). The number of cells showing nuclear and cytoplasmic Venus fluorescence in cells transfected with CFP-TAP was approximately four times greater than that of cells with exclusively nuclear Venus fluorescence, as determined by counting 15 fields of cells. This indicates that NC-Venus-ICP27 is able to function-

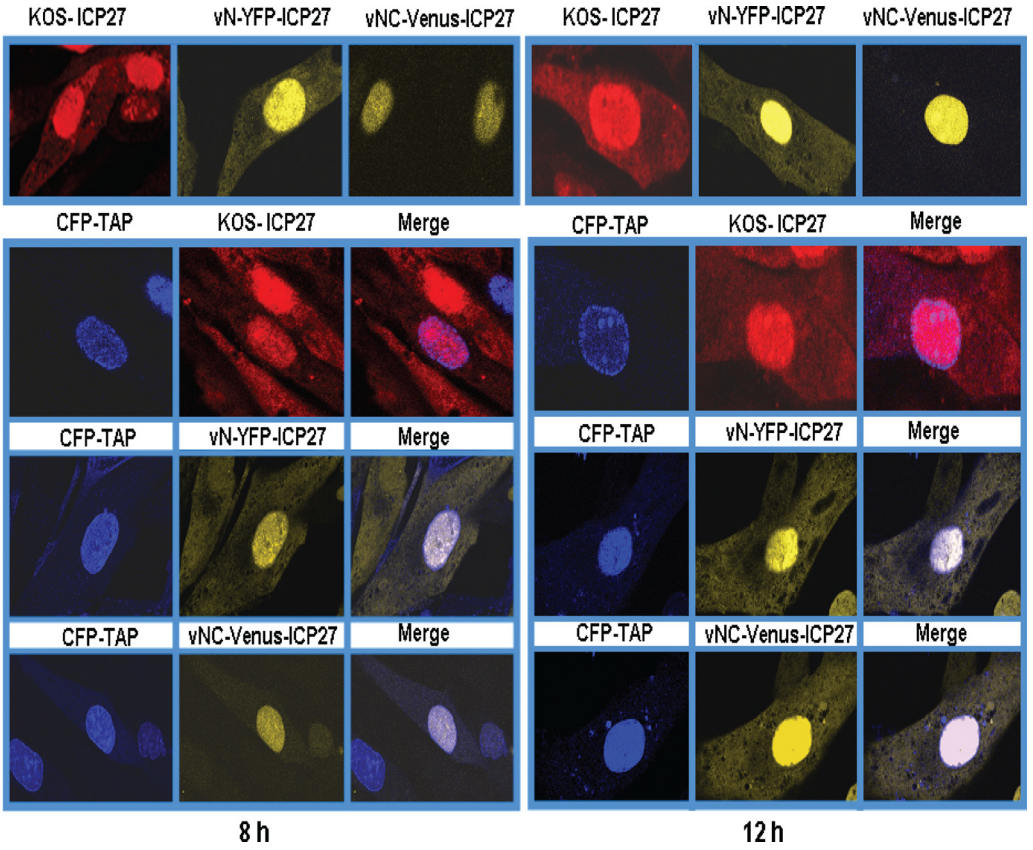

FIG. 8. Overexpression of TAP/NXF1 results in the export of NC-Venus-ICP27 to the cytoplasm. RSF cells either were not transfected or were transfected with CFP-TAP DNA as indicated. Twenty-four hours later, cells were infected with KOS, vN-YFP-ICP27, and v-NC-Venus-ICP27 at an MOI of 10. Cells were fixed at 8 and 12 h after infection. KOS-infected cells were stained with anti-ICP27 antibody, and CFP, YFP, and Venus fluorescence were visualized directly.

ally interact with TAP/NXF1, although much less efficiently than wild-type ICP27. It is, in fact, possible that the interaction with TAP/NXF1 occurred in a subset of NC-Venus-ICP27 molecules before BiFC occurred in this subset, which would lock ICP27 in a head-to-tail configuration that might preclude interaction with TAP/NXF1. BiFC could have occurred in this subset of ICP27 molecules that were exported after they reached the cytoplasm.

DISCUSSION

ICP27 is a multifunctional protein that undergoes a multitude of interactions throughout the course of infection (36). A number of these interactions involve both the N and C termini of ICP27, while others require internal regions of the protein. An important question is how the numerous interactions of ICP27 are regulated. ICP27 undergoes two posttranslational modifications, phosphorylation (47) and arginine methylation (26). We have reported that arginine methylation affects ICP27's export and its interactions with two of its interacting proteins, SRPK1 and Aly/REF (42, 43), but arginine methylation within the RGG box RNA binding domain does not affect RNA binding by ICP27 (K. Corbin-Lickfett, S. K. Souki, and R. M. Sandri-Goldin, unpublished results). ICP27 phosphorylation site mutants also were unable to interact with several proteins (9, 34). Some cellular proteins have been shown to fold into a head-to-tail conformation that can inhibit interactions with ligands or other proteins (7, 11, 22, 27, 28, 28, 44, 46). For example, NHERF1/EBP50 folds in a head-to-tail conformation that inhibits the interaction of its PDZ domains with ligands (28). The scaffold protein PDZK1 undergoes a head-to-tail intramolecular interaction that negatively regulates its interaction with EBP50 (22), and the ATPase activity of kinesin-1 motor protein is regulated by a direct interaction of its head and tail (22). We postulated that ICP27 undergoes a head-to-tail intramolecular interaction, which was demonstrated to be the case here using BiFC and FRET by acceptor photobleaching. The N-terminal leucine-rich region and the C-terminal zinc finger region must be intact for this to occur.

In these studies, the renaturation of the Venus protein occurs via covalent bonding, and therefore, ICP27 becomes locked in the head-to-tail conformation. This apparently hinders its interaction with RNAP II and TAP/NXF1, both of which require the N and C termini of ICP27 for interaction. As a consequence, vN-Venus-ICP27 virus replication is severely defective. In wild-type KOS infection, ICP27 may exist in open and closed states such that interaction with other proteins occurs when the head and tail are in proximity but are in an open state, whereas the closed state would preclude some protein interactions. It also is possible that wild-type ICP27

mostly exists in a head-to-tail configuration during infection, but in NC-Venus-ICP27 the presence of Venus may cause a steric hindrance that prevents other proteins from accessing ICP27. One surprising finding from these studies was that ICP27 apparently cannot undergo intermolecular head-to-tail interactions that would result in dimer formation. We previously reported that ICP27 can form dimers or multimers during infection (48). However, in this report we found that intermolecular head-to-tail interaction did not occur in the BiFC assays or using FRET by acceptor photobleaching. It still is possible that the NC-Venus-ICP27 protein forms a dimer by the head-to-tail interactions of two molecules of NC-Venus-ICP27, as was shown for HSV-1 UL9 (4). We will be performing native gels to determine if this occurs. However, in the competition experiment (Fig. 3), wild-type ICP27 expressed during KOS infection did not interfere with BiFC of N-Venus/ICP27/C-Venus, as would have been expected if wild-type ICP27 could form head-to-tail dimers with N-Venus/ICP27/C-Venus. It is possible that the Venus protein fragments fused to ICP27 interfered with dimer formation by some sort of masking of ICP27 domains, but if that were the case, we would not have observed BiFC or FRET, which we did. It also is possible that the head-to-tail intramolecular interaction must be disrupted for the formation of dimers or multimers that may form as part of ICP27's numerous functions. Again, locking the molecule in the head-to-tail configuration by BiFC would prevent that from occurring.

In sum, we demonstrated here that ICP27 can undergo a head-to-tail intramolecular interaction, and this may regulate its interactions with several proteins, as has been found for a number of cellular proteins. We currently are investigating how intramolecular association affects ICP27's interactions with the full range of its binding partners.

ACKNOWLEDGMENTS

We thank Atsushi Miyawaki for the Venus construct (29).

This work was supported by National Institute of Allergy and Infectious Diseases grant AI61397.

REFERENCES

1. **Bachi, A., I. C. Braun, J. P. Rodrigues, N. Pante, K. Ribbeck, C. von Kobbe, U. Kutay, M. Wilm, D. Gorlich, M. Carmo-Fonseca, and E. Izaurralde.** 2000. The C-terminal domain of TAP interacts with the nuclear pore complex and promotes export of specific CTE-bearing RNA substrates. RNA **6:**136–158.
2. **Bryant, H. E., S. Wadd, A. I. Lamond, S. J. Silverstein, and J. B. Clements.** 2001. Herpes simplex virus IE63 (ICP27) protein interacts with spliceosome-associated protein 145 and inhibits splicing prior to the first catalytic step. J. Virol. **75:**4376–4385.
3. **Burch, A. D., and S. K. Weller.** 2004. Nuclear sequestration of cellular chaperone and proteasomal machinery during herpes simplex virus type 1 infection. J. Virol. **78:**7175–7185.
4. **Chattopadhyay, S., and S. K. Weller.** 2007. Direct interaction between the N- and C-terminal portions of the herpes simplex virus type 1 origin binding protein UL9 implies the formation of a head to tail dimer. J. Virol. **81:**13659–13667.
5. **Chen, I. B., L. Li, L. Silva, and R. M. Sandri-Goldin.** 2005. ICP27 recruits Aly/REF but not TAP/NXF1 to herpes simplex virus type 1 transcription sites although TAP/NXF1 is required for ICP27 export. J. Virol. **79:**3949–3961.
6. **Chen, I. B., K. S. Sciabica, and R. M. Sandri-Goldin.** 2002. ICP27 interacts with the export factor Aly/REF to direct herpes simplex virus 1 intronless RNAs to the TAP export pathway. J. Virol. **76:**12877–12889.
7. **Chong, H., and K. Guan.** 2003. Regulation of Raf through phosphorylation and N terminus-C terminus interaction. J. Biol. Chem. **218:**36269–36276.
8. **Corbin-Lickfett, K., I. B. Chen, M. J. Cocco, and R. M. Sandri-Goldin.** 2009. The HSV-1 ICP27 RGG box specifically binds flexible, GC-rich sequences but not G-quartet structures. Nucleic Acids Res. **37:**7290–7301.
9. **Corbin-Lickfett, K., S. Rojas, L. Li, M. J. Cocco, and R. M. Sandri-Goldin.** 2010. ICP27 phosphorylation site mutants display altered functional interactions with cellular export factors Aly/REF and TAP/NXF1 but are able to bind herpes simplex virus 1 RNA. J. Virol. **84:**2212–2222.
10. **Dai-Ju, J. Q., L. Li, L. A. Johnson, and R. M. Sandri-Goldin.** 2006. ICP27 interacts with the C-terminal domain of RNA polymerase II and facilitates its recruitment to herpes simplex virus-1 transcription sites, where it undergoes proteasomal degradation during infection. J. Virol. **80:**3567–3581.
11. **Dietrich, K. A., C. V. Sindelar, P. D. Brewer, K. H. Downing, C. R. Cremo, and S. E. Rice.** 2008. The kinesin-1 motor protein is regulated by a direct interaction of its head and tail. Proc. Natl. Acad. Sci. USA **105:**8938–8943.
12. **Dueber, J. E., B. J. Yeh, R. P. Bhattacharyya, and W. A. Lim.** 2004. Rewiring cell signaling: the logic and plasticity of eukaryotic protein circuitry. Curr. Opin. Struct. Biol. **14:**690–699.
13. **Ellison, K. S., R. A. Maranchuk, K. L. Mottet, and J. R. Smiley.** 2005. Control of VP16 translation by the herpes simplex virus type 1 immediate-early protein ICP27. J. Virol. **79:**4120–4131.
14. **Fontaine-Rodriquez, E. C., and D. M. Knipe.** 2008. Herpes simplex virus ICP27 increases translation of a subset of viral late mRNAs. J. Virol. **82:**3538–3545.
15. **Fontaine-Rodriguez, E. C., T. J. Taylor, M. Olesky, and D. M. Knipe.** 2004. Proteomics of herpes simplex virus infected cell protein 27: association with translation initiation factors. Virology **330:**487–492.
16. **Hu, C. D., Y. Chinenov, and T. K. Kerppola.** 2002. Visualization of interactions among bZIP and Rel family proteins in living cells using bimolecular fluorescence complementation. Mol. Cell **9:**796–798.
17. **Johnson, L. A., L. Li, and R. M. Sandri-Goldin.** 2009. The cellular RNA export receptor TAP/NXF1 is required for ICP27-mediated export of herpes simplex virus 1 RNA, whereas the TREX-complex adaptor protein Aly/REF appears to be dispensable. J. Virol. **83:**6335–6346.
18. **Karpova, T., and J. G. McNally.** 2006. Detecting protein-protein interactions with CFP-YFP FRET by acceptor photobleaching. Curr. Protoc. Cytom. **12:**12–17.
19. **Kerppola, T. K.** 2006. Visualization of molecular interactions by fluorescence complementation. Nat. Rev. Mol. Cell Biol. **7:**449–456.
20. **Kerppola, T. K.** 2009. Visualization of molecular interactions using bimolecular fluorescence complementation analysis: characteristics of protein fragment complementation. Chem. Soc. Rev. **38:**2876–2886.
21. **Koffa, M. D., J. B. Clements, E. Izaurralde, S. Wadd, S. A. Wilson, I. W. Mattaj, and S. Kuersten.** 2001. Herpes simplex virus ICP27 protein provides viral mRNAs with access to the cellular mRNA export pathway. EMBO J. **20:**5769–5778.
22. **LaLonde, D. P., and A. Bretscher.** 2009. The scaffold protein PDZK1 undergoes a head to tail intramolecular association that negatively regulates its interaction with EBP50. Biochemistry **48:**2261–2271.
23. **Lengyel, J., C. Guy, V. Leong, S. Borge, and S. A. Rice.** 2002. Mapping of functional regions in the amino-terminal portion of the herpes simplex virus ICP27 regulatory protein: importance of the leucine-rich nuclear export signal and RGG box RNA-binding domain. J. Virol. **76:**11866–11879.
24. **Li, L., L. A. Johnson, J. Q. Dai-Ju, and R. M. Sandri-Goldin.** 2008. Hsc70 focus formation at the periphery of HSV-1 transcription sites requires ICP27. PLoS One **3:**e1491.
25. **Livingston, C. M., M. F. Ifrim, A. E. Cowan, and S. K. Weller.** 2009. Virus-induced chaperone-enriched (VICE) domains function as nuclear protein quality control centers during HSV-1 infection. PLoS Pathog. **5:**e1000619.
26. **Mears, W. E., and S. A. Rice.** 1996. The RGG box motif of the herpes simplex virus ICP27 protein mediates an RNA-binding activity and determines in vivo methylation. J. Virol. **70:**7445–7453.
27. **Moody, J. D., J. Grange, M. P. A. Ascione, D. Boothe, E. Bushnell, and M. D. H. Hansen.** 2009. A zyxin head to tail interaction regulates zyxin-VASP complex formation. Biochem. Biophys. Res. Commun. **378:**625–628.
28. **Morales, F. C., Y. Takahashi, S. Momin, H. Adams, X. Chen, and M. Georgescu.** 2007. NHERF1/EBP50 head to tail intramolecular interaction masks association with PDZ domain ligands. Mol. Cell. Biol. **27:**2527–2537.
29. **Nagai, T., K. Ibata, E. S. Park, M. Kubota, K. Mikoshiba, and A. Miyawaki.** 2002. A variant of yellow fluorescent protein with fast and efficient maturation for cell-biological applications. Nat. Biotechnol. **20:**87–90.
30. **Olesky, M., E. E. McNamee, C. Zhou, T. J. Taylor, and D. M. Knipe.** 2005. Evidence for a direct interaction between HSV-1 ICP27 and ICP8 proteins. Virology **331:**94–105.
31. **Pufall, M. A., and B. J. Graves.** 2002. Autoinhibitory domains: modular effects of cellular regulation. Annu. Rev. Cell Dev. Biol. **18:**421–462.
32. **Rice, S. A., M. C. Long, V. Lam, and C. A. Spencer.** 1994. RNA polymerase II is aberrantly phosphorylated and localized to viral replication compartments following herpes simplex virus infection. J. Virol. **68:**988–1001.
33. **Roberts, G. C. K., and D. R. Critchley.** 2009. Structural and biophysical properties of the integrin-associated cytoskeletal protein talin. Biophys. Rev. **1:**61–69.
34. **Rojas, S., K. Corbin-Lickfett, L. Escudero-Paunetto, and R. M. Sandri-Goldin.** 2010. ICP27 phosphorylation site mutants are defective in herpes simplex virus 1 replication and gene expression. J. Virol. **84:**2200–2211.
35. **Sandri-Goldin, R. M.** 1998. ICP27 mediates herpes simplex virus RNA

export by shuttling through a leucine-rich nuclear export signal and binding viral intronless RNAs through an RGG motif. Genes Dev. **12:**868–879.
36. **Sandri-Goldin, R. M.** 2008. The many roles of the regulatory protein ICP27 during herpes simplex virus infection. Front. Biosci. **13:**5241–5256.
37. **Sciabica, K. S., Q. J. Dai, and R. M. Sandri-Goldin.** 2003. ICP27 interacts with SRPK1 to mediate HSV-1 inhibition of pre-mRNA splicing by altering SR protein phosphorylation. EMBO J. **22:**1608–1619.
38. **Sekulovich, R. E., K. Leary, and R. M. Sandri-Goldin.** 1988. The herpes simplex virus type 1 alpha protein ICP27 can act as a trans-repressor or a trans-activator in combination with ICP4 and ICP0. J. Virol. **62:**4510–4522.
39. **Shyu, Y. J., H. Liu, X. Deng, and C. D. Hu.** 2006. Identification of new fluorescent protein fragments for bimolecular fluorescence complementation analysis under physiological conditions. Biotechniques **40:**61–66.
40. **Smith, I. L., M. A. Hardwicke, and R. M. Sandri-Goldin.** 1992. Evidence that the herpes simplex virus immediate early protein ICP27 acts post-transcriptionally during infection to regulate gene expression. Virology **186:**74–86.
41. **Soliman, T. M., R. M. Sandri-Goldin, and S. J. Silverstein.** 1997. Shuttling of the herpes simplex virus type 1 regulatory protein ICP27 between the nucleus and cytoplasm mediates the expression of late proteins. J. Virol. **71:**9188–9197.
42. **Souki, S. K., P. D. Gershon, and R. M. Sandri-Goldin.** 2009. Arginine methylation of the ICP27 RGG box regulates ICP27 export and is required for efficient herpes simplex virus 1 replication. J. Virol. **83:**5309–5320.
43. **Souki, S. K., and R. M. Sandri-Goldin.** 2009. Arginine methylation of the ICP27 RGG box regulates the functional interactions of ICP27 with SRPK1 and Aly/REF during herpes simplex virus 1 infection. J. Virol. **83:**8970–8975.
44. **Umeki, N., H. S. Jung, S. Watanabe, T. Sakai, X. Li, R. Ikebe, R. Craig, and M. Ikebe.** 2009. The tail binds to the head-neck domain, inhibiting ATPase activity of myosin VIIA. Proc. Natl. Acad. Sci. USA **106:**8483–8488.
45. **Wadd, S., H. Bryant, O. Filhol, J. E. Scott, T.-Y. Hsieh, R. D. Everett, and J. B. Clements.** 1999. The multifunctional herpes simplex virus IE63 protein interacts with heterogeneous ribonucleoprotein K and with casein kinase 2. J. Biol. Chem. **274:**28991–28998.
46. **Wong, Y. L., K. A. Dietrich, N. Naber, R. Cooke, and S. E. Rice.** 2009. The kinesin-1 tail conformationally restricts the nucleotide pocket. Biophys. J. **96:**2799–2807.
47. **Zhi, Y., and R. M. Sandri-Goldin.** 1999. Analysis of the phosphorylation sites of the herpes simplex virus type 1 regulatory protein ICP27. J. Virol. **73:**3246–3257.
48. **Zhi, Y., K. S. Sciabica, and R. M. Sandri-Goldin.** 1999. Self interaction of the herpes simplex virus type 1 regulatory protein ICP27. Virology **257:**341–351.
49. **Zhou, C., and D. M. Knipe.** 2002. Association of herpes simplex virus 1 ICP8 and ICP27 with cellular RNA polymerase II holoenzyme. J. Virol. **76:**5893–5904.